

SUPPORTING INFORMATION

Cargo-shell and cargo-cargo couplings govern the mechanics of artificially-loaded virus-derived cages

Aida Llauró¹, Daniel Luque^{2,3}, Ethan Edwards⁴, Benes L. Trus⁵, John Avera⁴, David
Reguera⁶, Trevor Douglas⁴, Pedro J. de Pablo^{1,7*}, José R. Castón^{2,*}

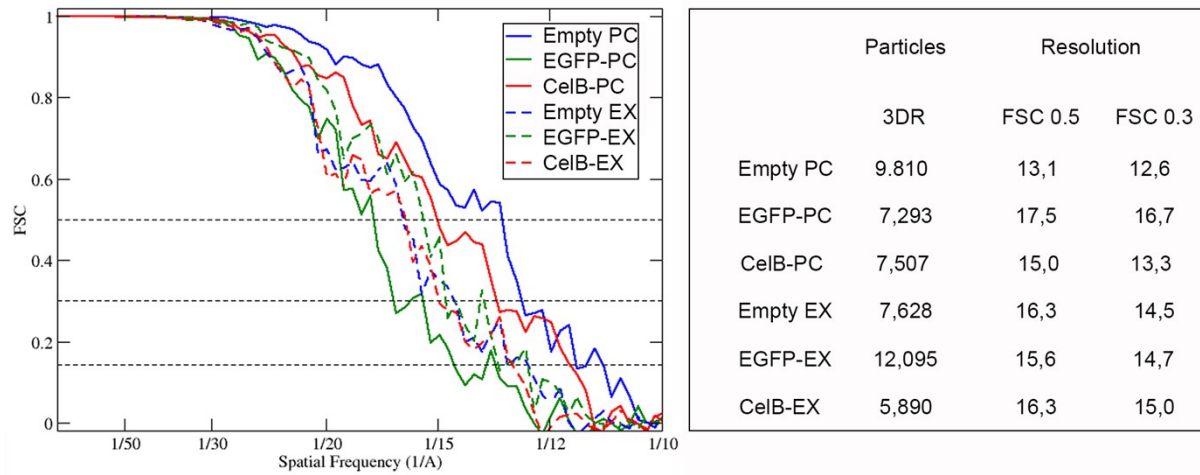


Figure S1. Resolution of empty procapsid (PC), EGFP- and CelB-PC, empty expanded particles (EX), EGFP- and CelB-EX. Fourier shell correlation (FSC) resolution curves were calculated for empty PC (blue), EGFP-PC (green), CelB-PC (red), empty EX (dashed blue), EGFP-EX (dashed green) and CelB-EX (dashed red). Number of particles included in the 3DR, and resolutions based on 0.5 and 0.3 criteria are indicated.

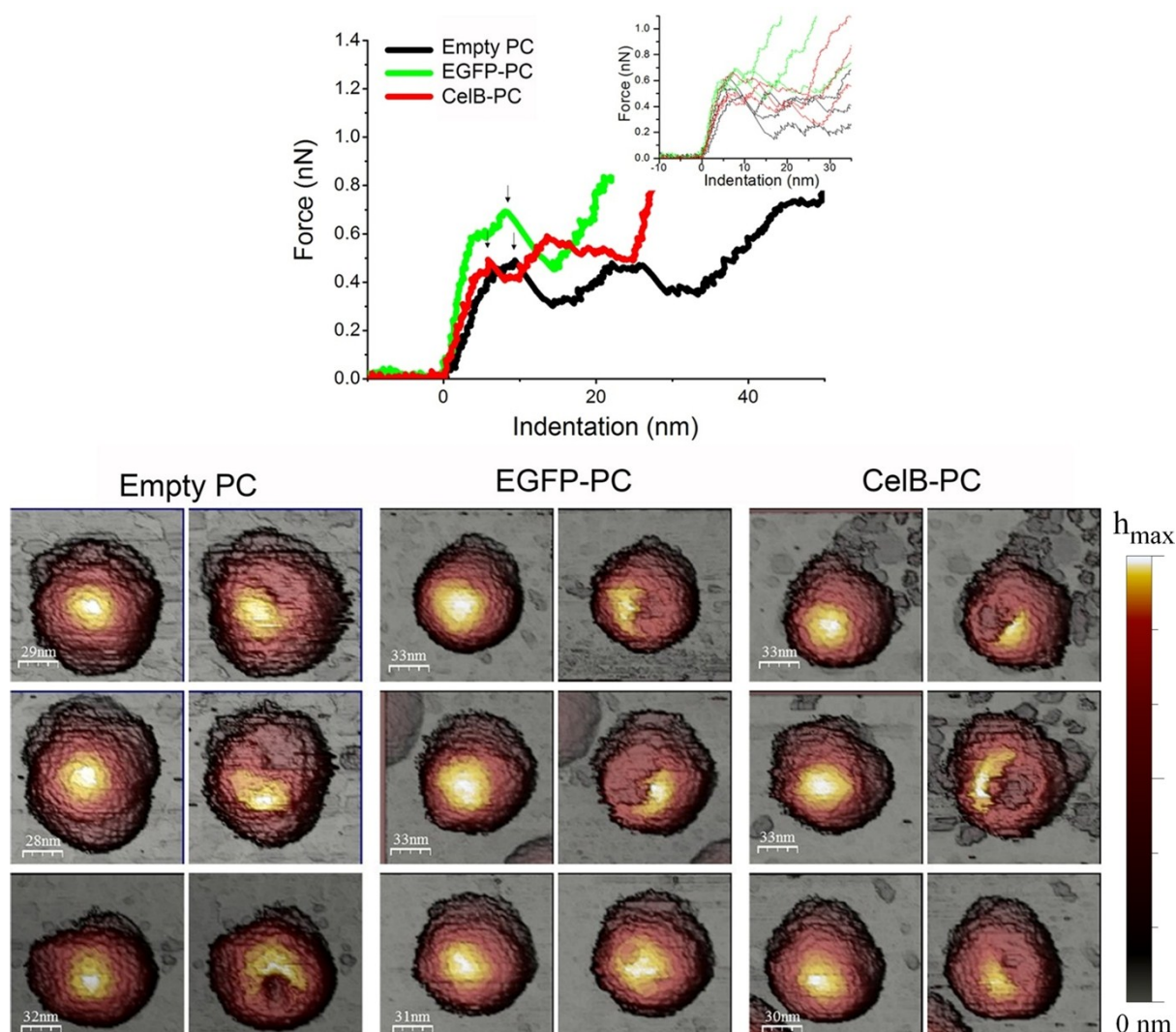


Figure S2. AFM nanoindentation on empty and loaded PC. (Top) Comparison of three typical nanoindentation curves for an empty PC (black), EGFP-PC (green) and CelB-PC (red). We observed a non-linear regime before particle breakage (arrows). (Inset) Other examples of PC FIC. (Bottom) AFM images of PC before (left) and after a single nanoindentation (right). Images show clear damage to the particle shell. Each image was normalized to its maximum height.

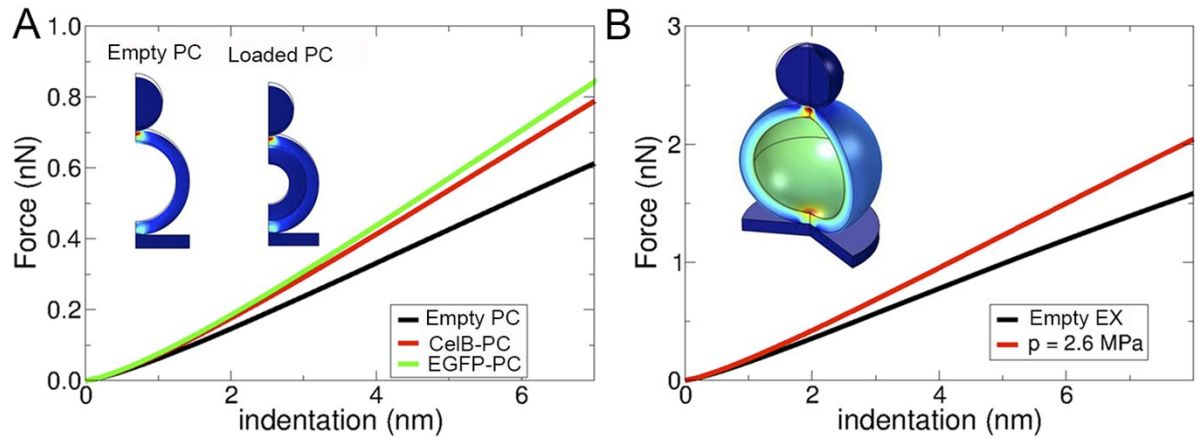


Figure S3. (A) Force-indentation curves obtained from Finite Element Simulations that mimic AFM experiments for PC. The empty PC is represented as a spherical shell with an external radius $R = 29.8$ nm and 7.5 nm thickness, indented on a hard substrate by a spherical tip with radius $R_{in} = 15$ nm. The Young modulus of the PC was $E = 58$ MPa, chosen to yield the same spring constant value as in experiments for empty PC. The cargo effect is modeled by addition of a second, 10-nm-thick layer (2D transverse sections, inset). The graph shows the values for the empty PC (black line); CelB-PC (red) and EGFP-PC (green) are shown with a second internal layer of $E = 6$ and $E = 8$ MPa, respectively. (B) Force-indentation curves obtained from Finite Element Simulations that mimic the AFM experiments for EX. The graph shows the values for an unpressurized empty EX (black line) and an EX (red) with an internal pressure of 2.6 MPa. The inset shows the model used for simulations, where EX is shown as a 6.6-nm-thick spherical shell with an external radius $R = 32.4$ nm, indented on a hard substrate by a spherical tip with a radius $R_{in} = 15$ nm. The Young modulus of the capsid was $E = 178$ MPa, chosen to yield the same spring constant value as in experiments for empty EX.

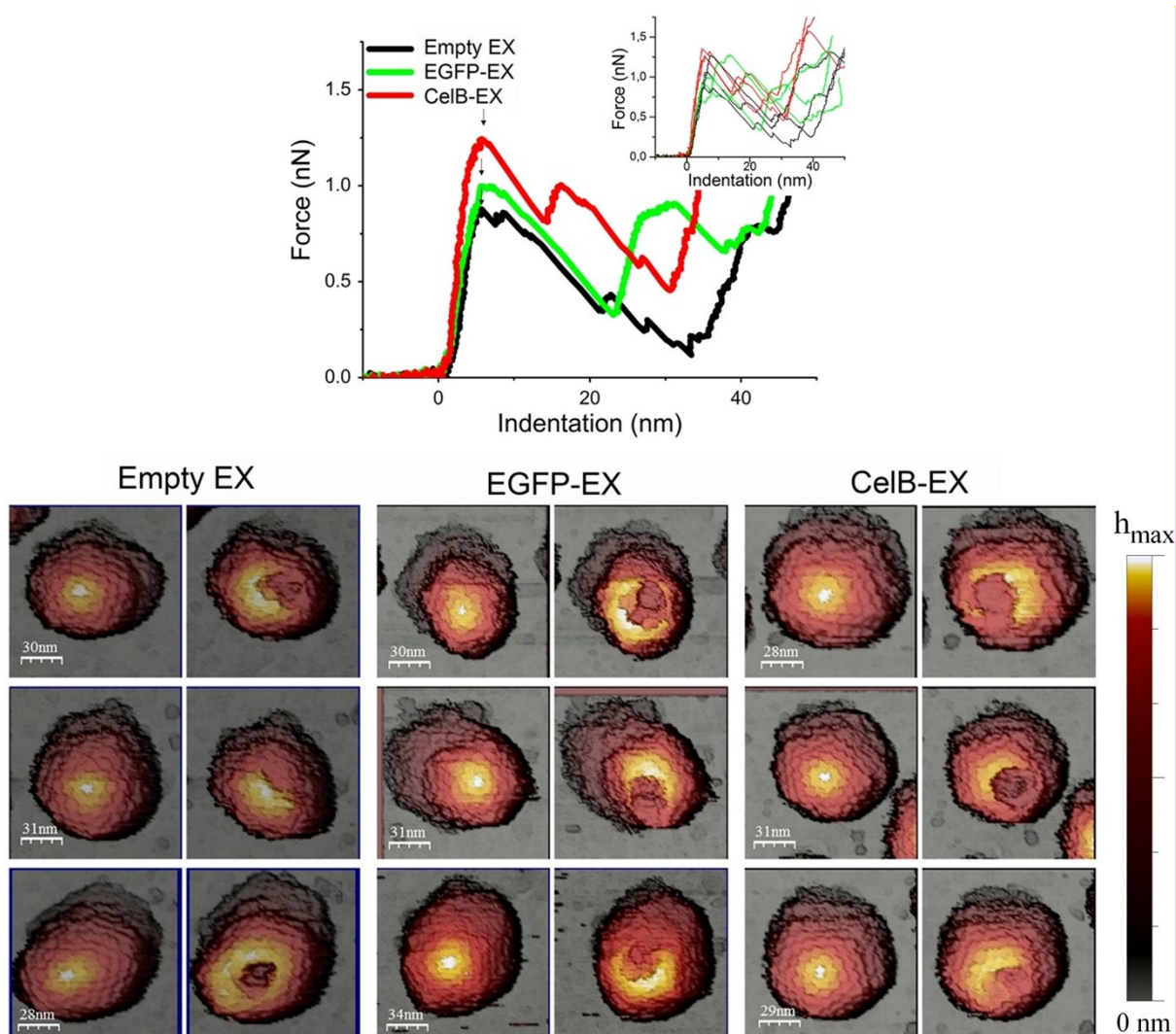


Figure S4. AFM nanoindentation on empty and loaded EX. (Top) Comparison of three typical nanoindentation curves for an empty EX (black), EGFP-EX (green) and CelB-EX (red). Particle breakage is indicated (arrows). (Inset) Other examples of EX FIC. (Bottom) AFM images of EX before (left) and after a single nanoindentation (right). Images show loss of some capsid subunits. Each image was normalized to its maximum height.

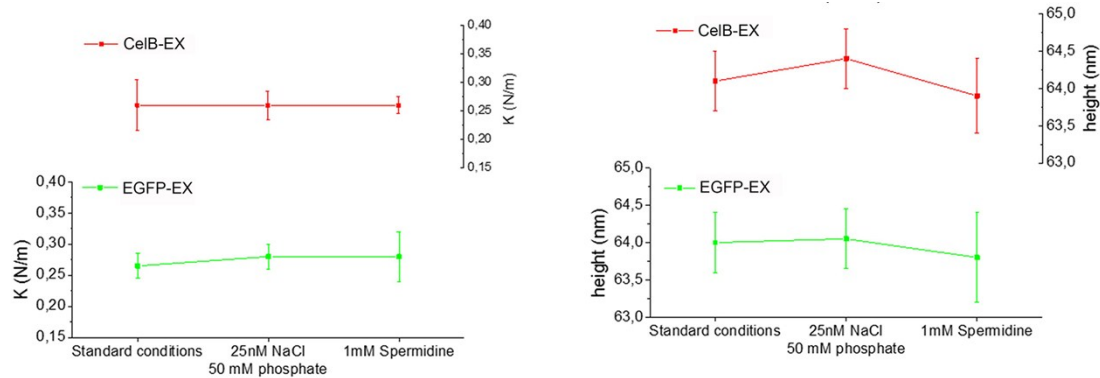


Figure S5. AFM indentations of CelB- and EGFP-EX in different buffers. We tested the effect of electrostatic interactions on cargo-loaded EX rigidity at low ionic strength (50 mM phosphate, 25 mM NaCl, pH 7) or in the presence of spermidine (100 mM phosphate, 50 mM NaCl, 1 mM spermidine, pH 7) compared to standard conditions (100 mM phosphate, 50 mM NaCl, pH 7). EGFP- and CelB-EX were tested similarly; each sample was incubated in standard buffer and its elastic constant measured by AFM, followed by buffer exchange first to lower ionic strength and then to spermidine buffer. No significant differences were found (Table S3). (A, B) Average elastic constant (A) and average height (B) of CelB-EX (red) and EGFP-EX (green) in different buffer conditions.

Table S1. Mechanical characterization of empty and loaded P22 PC and EX

	Particles (n°)	Breaking force (nN)	K(N/m)	$\epsilon_{\text{critical}}$	Height (nm)	Relative deformation
Empty PC	32	0.56 ± 0.02	0.094 ± 0.006	0.18 ± 0.01	50 ± 1	0.86
EGFP-PC	35	0.68 ± 0.03	0.131 ± 0.005	0.17 ± 0.01	56.3 ± 0.5	0.97
CelB-PC	25	0.54 ± 0.03	0.12 ± 0.01	0.14 ± 0.01	56.5 ± 0.7	0.98
Empty EX	24	1.02 ± 0.05	0.21 ± 0.01	0.13 ± 0.01	58 ± 1	0.91
CelB-EX	24	1.20 ± 0.07	0.27 ± 0.03	0.13 ± 0.01	63.3 ± 0.8	0.98
EGFP-EX	21	1.11 ± 0.05	0.27 ± 0.01	0.13 ± 0.01	62.7 ± 0.3	0.98

The values show mean \pm SE of single particles. Breaking force is the maximum force reached before breakage. The elastic constant was determined by linear adjustment of the initial part of the FIC. Critical strain ($\epsilon_{\text{critical}}$) was calculated by dividing critical indentation by height. Particle height was determined from a profile of the center of its image. Relative deformation is the ratio of AFM height to nominal size from 3DR cryo-EM.

Table S2. Volume and charge of P22 PC, EX and their cargos

	Volume ^a (nm ³)	Total cargo volume (nm ³)	Shell thickness (nm)	Net surface charge ^b (e)
PC	46,452 ^c		7.5	-
EX	71,936 ^d		6.6	-840 ^j
CelB (tetramer)	581 ^e		-	-37 ^k
EGFP	55 ^f		-	0 ^l
C _t helix-loop-helix	4.2		-	5 ^m
SP N _t linker	15.8 ^g		-	2 ⁿ
CelB & 4 SP	661	21,152 ^h	-	-288
EGFP & 1 SP	75	16,800 ⁱ	-	+1586

^aMeasurements were obtained by 3D cryo-EM analysis

^bNet surface charges were calculated as indicated in the VIPERdb server (<http://vipierdb.scripps.edu>); basically, net surface charge is calculated by adding the charges of the inner surface-exposed positive (Lys, Arg, His) and negative (Glu, Asp) residues.

^cVolume when a perfect sphere is assumed, PC inner radius = 223 Å (outer radius = 298 Å).

^dVolume when a perfect sphere is assumed, EX inner radius = 258 Å (outer radius = 324 Å).

^eCelB tetramer dimensions: 101 x 101 x 57 Å

^fEGFP monomer dimensions: 48 x 33 x 35 Å

^gVolume occupied by the SP segment 141-263

^hVolume for 32 CelB tetramers

ⁱVolume for 224 EGFP monomers

^jThe EX asymmetric unit inner surface has a total charge of -14 e (39 Asp, 62 Glu, 23 Lys, 64 Arg).

^kThe CelB tetramer outer surface has 169 Asp, 283 Glu, 238 Lys, 92 Arg, and 85 His

^lThe EGFP outer surface contains 12 Asp, 12 Glu, 16 Lys, 6 Arg and 2 His

^mThe SP C_t helix-loop-helix motif has 7 Asp, 1 Glu, 7 Lys and 3 Arg

ⁿThe SP N_t linker (residues 141-263) has 6 Asp, 10 Glu, 9 Lys, 8 Arg and 2 His

Table S3. Elastic constant and height of CelB- and EGFP-EX in distinct ionic conditions

Buffer	CelB-EX			EGFP-EX		
	Particles (n°)	K (N/m)	Height (nm)	Particles (n°)	K (N/m)	Height (nm)
50 mM NaCl, 100 mM phosphate	9	0.26 ± 0.045	64.1 ± 0.4	4	0.27 ± 0.02	64 ± 0.4
25 mM NaCl, 50 mM phosphate	14	0.26 ± 0.025	64.4 ± 0.4	13	0.28 ± 0.02	64.05 ± 0.4
1 mM spermidine	17	0.26 ± 0.015	63.9 ± 0.5	7	0.28 ± 0.04	63.8 ± 0.6

Finite element simulations of P22 PC and EX

Finite elements simulations of AFM indentation of P22 were performed using the COMSOL Multiphysics 4.3 program (Comsol, Stockholm, Sweden). In all cases, the capsid wall was considered to be made of a homogenous material, using Young Modulus E and Poisson ratio $\nu = 0.3$ (a standard value for protein-like materials). This model capsid was placed on a hard flat substrate and indented by a hard spherical object with radius $R_{in} = 15$ nm to mimic the AFM tip. The system was simulated using a 2D axisymmetric model meshed with over 3000-6000 triangular elements. Contacts were implemented between the shell and the tip as well as the supporting surface during indentation with a contact-penalty stiffness method according to manufacturer's protocols. A parametric, non-linear solver was used to simulate the stepwise lowering of the tip onto the capsid. The spring constant was derived from a linear fit of force vs indentation for small indentations in the linear region between 2 and 6 nm.

The empty PC was modeled as a thick spherical shell with an external radius $R = 29.8$ nm and thickness $h = 7.5$ nm (Figure S2A, inset). The presence of cargo attached to the PC was modeled by adding a second layer beneath the capsid layer with a different Young's modulus and 10 nm thick (estimated from 3DR cryo-EM radial density profiles). The indentation curves obtained for the model PC with a $R_{in} = 15$ nm tip and Young modulus value $E = 58 \pm 4$ MPa, chosen to reproduce the experimental value of the empty PC spring constant (0.094 ± 0.006 N/m), is shown in Figure S2A. The indentation curves for two PC with the internal second (cargo) layer showed Young's modulus values of 6 MPa and 8 MPa, yielding spring constants of $k = 0.12$ and $k = 0.131$ N/m, identical to the experimental values measured for CelB-PC and EGFP-PC, respectively. The effective Young's modulus for the cargo is thus nearly 10 times smaller for CelB and 7 times smaller for EGFP than that of the PC shell.

The empty EX was modeled as a thick spherical shell with an external radius $R = 32.4$ nm and thickness $h = 6.6$ nm (Figure S2B, inset). Finite elements simulations were used to corroborate pressure estimates based on the Vela formula. Indentation curves for the model EX capsid with a $R_{in} = 15$ nm tip and a Young modulus value $E = 0.178 \pm 0.009$ GPa, chosen to reproduce the experimental spring constant value of empty EX (0.21 ± 0.01 N/m), are shown in Figure S2B. The indentation curve when EX internal pressure is 2.6 MPa, which yields a spring constant $k = 0.27$ N/m, is identical to the experimental value measured for the cargo-loaded EX. The estimated pressure in finite element simulations is thus 2.6 ± 1.1 MPa, compatible with the value obtained from the Vela formula (Eq. 1, main text).¹

Electrostatic contributions to osmotic pressure in EX

The cargo can be considered a solution of N effective charged spheres in an electrolyte with a Debye length given by the salt concentration of the buffer (100 mM phosphate, 50 mM NaCl, yielding $\kappa^{-1} = 0.796$ nm). Electrostatic repulsion between the cargo molecules is screened by the buffer salt and is described using the electrostatic repulsion part of the DLVO potential between two charged spheres; this allows calculation of the second virial coefficient B_2 , which quantifies the leading electrostatic contribution to the osmotic pressure. In the simplest approximation of treating the cargo as point charges,²

$$B_2 = \frac{z^2}{2\Sigma}$$

Where Σ is solvent ionic strength and z is the charge of cargo molecules, in elementary charge units. The resulting contribution to the osmotic pressure is

$$\Pi_{elec} = k_B T \rho^2 B_2$$

For CelB, with an estimated charge of 9 electrons ($Z = -9$; Table S2) per tetramer (which includes the SP charge),

$$p \approx k_B T \rho^2 B_2 = 180 Pa$$

For EGFP, with an estimated positive charge of 7 (Table S2),

$$p \approx k_B T \rho^2 B_2 = 5000 Pa$$

In both cases, this contribution is negligibly small and cannot explain the large pressure values derived in the nanoindentation experiments.

The electrostatic contribution to the osmotic pressure can also be estimated through the Donnan equilibrium, by which the chemical equilibrium between the capsid interior and exterior, with a fixed charge that cannot escape from the capsid, leads to a higher interior counterion concentration that is responsible for the osmotic pressure. The osmotic pressure here can be evaluated as described,³ to yield

$$\Delta\Pi = k_B T \left(\sqrt{n_0^2 - n_b^2} - 2n_b \right)$$

where n_0 is net charge density of the cargo and n_b is bulk salt density (~150 mM here). The

interior charge density can be estimated as $n_0 = \frac{zN}{V_{capsid} - V_{cargo}}$, where we subtract the volume

occupied by the cargo. For CelB with $z = -9$ per tetramer:

$$\Delta\Pi = k_B T \left(\sqrt{n_0^2 - n_b^2} - 2n_b \right) = 370 Pa$$

For EGFP with $z = 7$ per molecule:

$$\Delta\Pi = k_B T \left(\sqrt{n_0^2 - n_b^2} - 2n_b \right) = 9800 Pa$$

In this case, the electrostatic contribution is thus also negligibly small.

To summarize, the osmotic pressure is dominated by packing effects, since the electrostatic contribution is negligible. This was confirmed by AFM nanoindentations, which showed no change in the elastic constants, independently of the presence of spermidine (which further screens electrostatic interactions) or when ionic strength was reduced.

References

- 1 Vella, D., Ajdari, A., Vaziri, A. & Boudaoud, A. The indentation of pressurized elastic shells: from polymeric capsules to yeast cells. *J R Soc Interface* **9**, 448-455 (2012).
- 2 Hill, T. L. *An introduction to statistical thermodynamics*. (Courier Corporation, 2012).
- 3 Cordova, A., Deserno, M., Gelbart, W. M. & Ben-Shaul, A. Osmotic shock and the strength of viral capsids. *Biophys J* **85**, 70-74 (2003).